RSC Advances

ROYAL SOCIETY OF CHEMISTRY

www.rsc.org/advances

Cite this: DOI: 10.1039/c0xx00000x

www.rsc.org/xxxxxx

Communication

Pinning Mechanism of Advancing Sessile Droplet on Superhydrophobic Surfaces

Jun Wu [*a], Jun Xia [*a], Wei Lei [a], Bao-ping Wang [a]

Received (in XXX, XXX) Xth XXXXXXXXX 20XX, Accepted Xth XXXXXXXXX 20XX
DOI: 10.1039/b000000x

This study explores the working mechanism and the influence factor of the pinning effect of advancing sessile droplet on micropillared superhydrophobic surfaces. Our experimental result reflects that the pinning effect of the advancing droplet is determined by a new parameter, which is named the local triple-phase contact line (LTCL). The pinning force is proved proportionate to the maximal value of the LTCL attainable along the actual droplet boundary. Meanwhile, a theory model is built to well explain the pinning phenomena on various liquid/solid interfaces.

Superhydrophobic surfaces, exhibiting high water contact angles (>150°), have attracted a lot of interests for their extreme non-wetting property [1-5]. The droplet on the superhydrophobic surfaces can be either slippery or sticky, which is differentiated by the pinning phenomena of the moving droplet on the surfaces. On a slippery surface, a water droplet rolls off the surface once it is tilted [1]. Such water repellent property has found applications in self-cleaning [6], drag reduction [7], anti-icing [8], anti-biofouling [9] and anti-corrosion [10]. In contrast to the slippery surface, the water droplet sitting on the sticky ones does not roll off even if the surface is turned upside down [2]. Such sticky superhydrophobic surfaces have potential applications in liquid transportation [11], ink-jet printing [12], and microfluidic devices [13]. Therefore, these superhydrophobic surfaces are entirely different in nature and have received growing interests in distinct application fields. However, the existing researches on these pinning phenomena are not consistent and the mechanism of the pinning effect has not been clearly understood [14-20]. Some researchers claimed that the solid fraction is the dominant factor [15-16] while some others believed that the triple-phase contact line (TCL) is the dominant factor instead. [18-20] Settling this disagreement and determining the controlling mechanism of the phenomena will contribute greatly to the scientific world. In this study by comparing and analyzing the difference between the advancing contact angles and the predicted Cassie angles [21], we were able to gain a deeper understanding of pinning mechanism which could be used to predict the pinning phenomena on superhydrophobic surfaces.

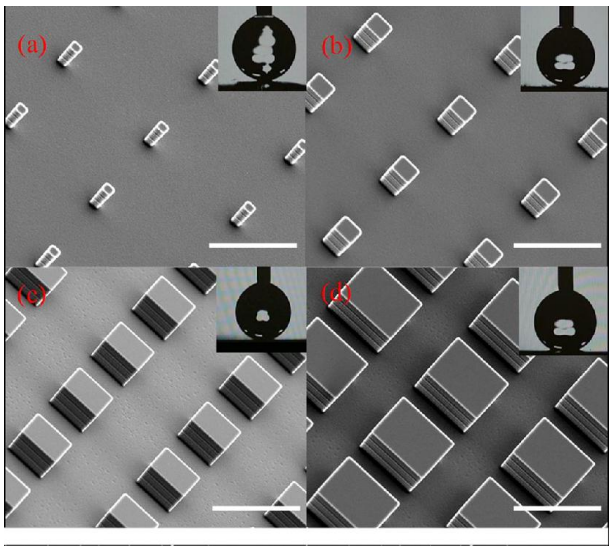

Fig. 1 Scanning electron microscopy images of the micropillared superhydrophobic surfaces. The solid fraction varies from (a) 0.01, (b) 0.04, (c) 0.16 to (d) 0.36. All scale bars are 40μm.

Fig. 1 shows the patterns fabricated by us. The micropillar patterns had the same pitch size (40 μm), but different side lengths of 4μm, 8μm, 16μm and 24μm. The solid fraction of these samples varied from 0.01, 0.04, and 0.16 to 0.36, denoted as S0.01, S0.04, S0.16 and S0.36, respectively. A flat silicon substrate was tested as a control experiment, and denoted as S1.00.

From the observation of apparent contact angles measurements by the sessile drop method (Method Section for details), the droplet boundary was fixed on the substrate in the initial stage and the contact radius of the droplet remained constant with increase of drop volume. This pinning mode was succeeded by a depinning mode once an increase of contact radius was observed. This pinning-depinning process was repeatly observed on every sample, as sketched in Fig. 2. As expected, the existence of the droplet pinning phenomenon indicated that there existed a pinning force on the liquid/solid interface. This explained why many metastable droplet profiles were observed with different apparent contact angles on the same superhydrophobic sample. During this whole

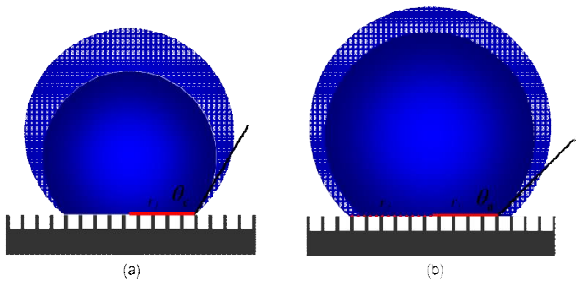

Fig. 2 The pinning and depinning phenomena of a volume growing water droplet on a patterned superhydrophobic surface in Cassie state. A (a) pinning mode transits to a (b) depinning mode during the volume growing process under the effect of a depinning force. θ_c is a thermodynamically stable contact angle in theory, θ_a is an advancing contact angle, and r is the contact radius of the droplet.

process, as the apparent contact angle increased, the driving force by surface tension opposing the pinning force per unit length of the apparent droplet boundary also got increased [22]. Once the apparent contact angle reaches to the largest value (the advancing contact angle θ_a), the driving force overcame the pinning force and lead to the depinning motion of the droplet boundary observed. The driving force therefore can be expressed as

$$F_d = \gamma(\cos\theta_c - \cos\theta_x) \quad (1)$$

where γ=72mN/m is the surface tension of water, θ_x ($\leqslant\theta_a$) and θ_c are the apparent contact angle and Cassie contact angle, respectively. Please note that the advancing contact angle θ_a is here defined as the largest apparent contact angle attainable.

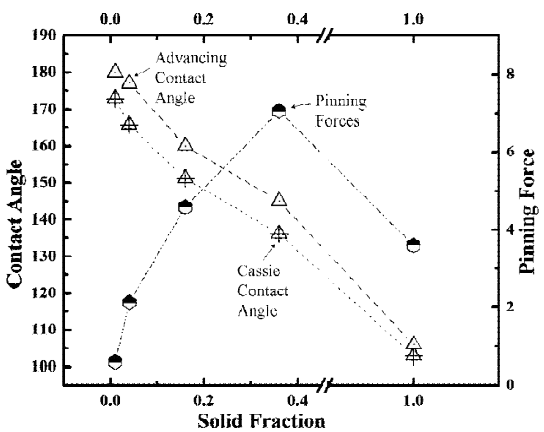

Fig. 3 The Cassie contact angles, the advancing contact angles and the pinning forces on the patterned superhydrophobic surfaces (S0.36, S0.16, S0.04 and S0.01) and a planar hydrophobic surface (S1.00)

Fig. 3 shows the predicted Cassie contact angles and the measured advancing contact angles of water droplet, and also the calculated pinning forces by submitting θ_a to Eq. (1), with respect to the liquid/solid contact area fraction. The results presented in Fig. 3 clearly indicated that the pinning force decreased with the liquid/solid contact area fraction on superhydrophobic surfaces. But S0.36 and S0.16 exhibited even greater pinning force than the one on hydrophobic smooth silicon surface. This result indicated that the patterned hydrophobic surfaces (i.e. low solid fraction) could cause a stronger pinning effect than a flat hydrophobic surface (i.e. unit solid fraction), and therefore, we believe that it is inappropriate to predict the pinning effect by simply using the parameter of liquid/solid contact area fraction. Coincidently, McCarthy supported that the role of TCL was much more important than liquid/solid contact area fraction in the pinning/depinning phenomena. [18-20] However, McCarthy studied the static and apparent TCL instead of the dynamic and actual TCL. Therefore, they still could not explain exactly how TCL affects the pinning phenomena.

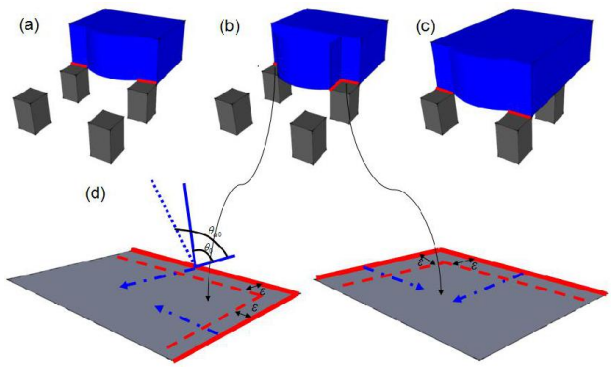

Fig. 4 The evolution of the LTCL with increasing droplet volume on a micropillared superhydrophobic surface, from (a) the initial contacting stage to (b) the pinning stage to (c) the depinning stage. (d) the sketch of the evolutionary process of local contact angles.

It is well-known that there are two interfaces, i.e. the liquid/solid interface and the liquid/air interface at the base of Cassie droplets [22]. Fluid is able to slip smoothly on the liquid/air interface [23]. Therefore, it can be concluded that the pinning force is caused by the liquid/solid interface. With this reasoning, let us describe the pinning/depinning process in Fig. 4. In our theory, once the droplet volume is increased to a certain value, the advancing boundary of the water droplet will depin from one row of pillars and quickly slip over the "air gap" between the pillars to the next row of pillars. During the initial contacting period, the LTCL occupies only one edge of the pillar due to the hydrophobic nature of the surface as indicated in red in Fig. 4(a). As the droplet volume increase, the discontinuous LTCL segments could not advance over the pillar surfaces immediately because of the local pinning force caused by the pillar edge, which is mainly induced by the inherent hysteresis of hydrophobic surface. Meanwhile, the boundary over the liquid/air interface advances freely to the spacing between pillars and gains new liquid/air interface underneath. During this stage, LTCL length is increased by elongation along the periphery of the pillars, which further increases the local pinning force on each pillar surface. This local pinning force increases until the spacing between the two adjacent pillars is totally replaced by the liquid/air interface, as indicated in Fig. 4(b). This local pinning effect

makes both the local contact angle θ_L at the LTCL and therefore the local driving force by surface tension increase with the droplet volume. Once the LTCL length reaches the maximal value and θ_L increases to the local inherent advancing contact angle value θ_{a0}, the maximal local driving force will appeal the depinning motion on each of the pillar surface. This makes the droplet boundary advance outwards and then slip over the "air gap" once again to contact the next pillars row, as indicated in Fig. 4(c) and (d). Briefly, the inherent hysteresis on hydrophobic surface resists the aggression of LTCL segments during the initial fluid volume increasing stage. However, after the local contact angle has reached the local inherent advancing contact angle value on the hydrophobic surface and the LTCL length is increased to a certain value, the local driving force on each pillar would overcome the local pinning force and realize the depinning motion.

The theory deduced above provides us an explanation of pinning phenomena on superhydrophobic surfaces from micro-perspective. Actually, this theory can also be utilized to predict the advancing contact angle. Let's assume an infinitesimally small displacement ε of the LTCL along the vector direction (Fig. 4(d)), the associated free energy change on each pillar can be calculated as

$$\mathrm{d}_{\mathrm{E}} = (\gamma_{SV} - \gamma_{SL}) X\varepsilon - \gamma\cos\theta_{a0} X\varepsilon \quad (2)$$

where X and ε indicate the LTCL length on each pillar and an infinitesimally small displacement, respectively. From Eq. (2), we can express the local driving force applied at the TCL on each pillar as

$$\mathrm{F}_{\mathrm{dm}} = \mathrm{d}_{\mathrm{E}} / \varepsilon = (\cos\theta_0 - \cos\theta_{a0})\gamma X \quad (3)$$

where θ_0 is obtained from the Yong's law [24], represents the local inherent contact angle. Note that Eq. (1) describes the driving force per unit length of the apparent droplet boundary. So we could obtain the advancing contact angle by combining Eq. (1) with Eq. (3)

$$\cos\theta_a = \cos\theta_c + \frac{(\cos\theta_{a0} - \cos\theta_0) X}{P} \quad (4)$$

where P represents the pitch of the adjacent pillars. In Eq. (4), X is the only unknown variable. In our theory, the LTCL elongation behavior is repeatable on those different square pillar arrays, which means all those pillar arrays share the same ratio value of X / L (where L is the square width). According to the analysis in the previous section, the fluid over the liquid/air interface will advance freely and occupy the whole spacing between adjacent pillar top endings. Therefore the maximal LTCL length attainable equals to 3/4 perimeter of the top surface, which means the ratio value of X / L is 3 in the case of square pillar structure. Then, the theoretical advancing contact angles could be obtained by submitting this value into Eq. (4). The comparisons between the theoretical and the experimental values of the advancing contact angles and the pinning force are presented in Fig.5. Fig. (5) indicate a very good fit between theoretical and experimental values, which corroborates our theory on the LTCL elongation behavior. Meanwhile, we could conclude that the critical influence factor for the pinning phenomena is the LTCL length.

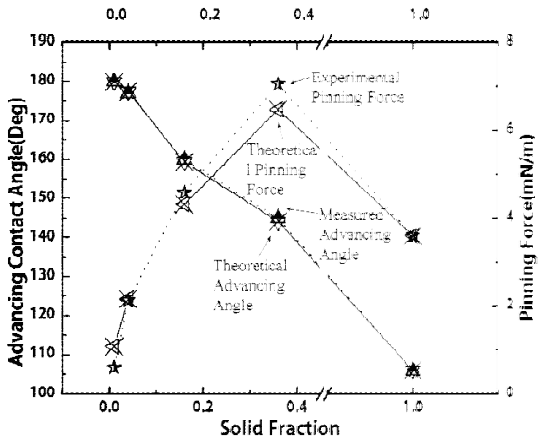

Fig. 5 Comparisons between the theoretical and experimental values of the advancing contact angles and the pinning forces. Experimental pinning forces are the values calculated from the measured advancing contact angles, while the theoretical pinning forces are the values predicted from Eq. (4).

We have further extended this theory to explain the stickiness of different surfaces. Let us define a new parameter δ and name it as the normalized LTCL length

$$\delta = \frac{X}{P} \quad (5)$$

The pinning/driving force is then related to this parameter as

$$F_{\mathrm{d}} = \delta\gamma(\cos\theta_0 - \cos\theta_{a0}) \quad (6)$$

Eq. (6) indicates that the pinning/driving force applied on unit length could be directly predicted by the normalized TCL length δ. It is obviously that the value of δ equal to unit on a flat surface since there is no LTCL elongation. On the contrary, the value of δ could be larger than unit on some superhydrophobic surfaces, such as S0.36 and S0.16. Therefore, the pinning/driving force is reasonable stronger than that on a flat hydrophobic surface. Meanwhile, a lower pinning/driving force is expected on S0.04 and S0.01.

This new built theory not only well explained the results in Fig. (3), but also could be used to explain the stickiness on other superhydrophobic surfaces. [15-16] We further extended the theory on the lotus leaf and rose petal, which represent the most famous examples of slippery and sticky superhydrophobic surfaces in nature, respectively. As only few nanoscale bumps over microstructure on lotus leaf is in contact with liquid, the LTCL elongation behavior is therefore well restricted. This results in a slippery surface according to our theory. In another case, the hierarchical micro- and nanostructures on the surface of rose petal make the liquid film impregnate into the gaps between microstructure, while holds a non-wetting state on nanostructure. The liquid film between microstructure makes the δ value on rose petal much greater than unit; the sticky performance also gets well explanation by using our model, and again proves the

applicability of our new theory. Actually, our finding is not only of interest in theory, but also of great interest in some real application fields, especially in the field of microfluidics. Droplet pinning mechanism could be well used to deposit biofluids, and then get biomaterials arranged in order. Therefore, results of this work can be applied for making novel microfluidic chips which can be used for studying biochemical and biophysical problems.

By investigating the advancing contact angles and analyzing the LTCL elongation behavior on different square pillar arrays, we found that the pinning force at the droplet boundary was directly proportional to the maximal LTCL attainable, which depends on the surface morphology. This new insight was used to explain the sticky or slippery behavior on various surfaces. This pinning mechanism is also important for making novel microfluidics operating platform, which features drag reduction or adhesive functions.

Notes and references

[a] *School of Electronic Science and Engineering, Southeast University, Nanjing 210096, China. Fax: +86-25-83792662; Tel: +86-25-83792650; E-mail: lancejunwu@gmail.com; xiajun@seu.edu.cn*

† Electronic Supplementary Information (ESI) available: [Experimental procedure]

1. W. Barthlott and C. Neinhuis, *Planta*, 1997, **202**, 1-8.
2. L. Feng, Y. A. Zhang, J. M. Xi, Y. Zhu, N. Wang, F. Xia and L. Jiang, *Langmuir* 2008, **24**,4114-4119.
3. N. Yi, B. Huang, L. N. Dong, X. J. Quan. F. J. Hong, P. Tao, C. Y. Song, W. Shang and T. Deng, *Sci. Rep.* 2014, **4**,4303.
4. X. Y. Jiang, Y. C. Wu, B. Su, R. G. Xie, W. S. Yang and L. Jiang, *Small* 2014, **10**, 258-264.
5. W. Da, S. J. Kim, W. K. Weong, S. H. Kim, K. R. Lee, H. Y. Kim and M. W. Moon, *Sci. Rep.* 2013, **3**, 2524.
6. R. Furstner, W. Barthlott, C. Neinhuis and P. Walzel, *Langmuir* 2005, **21**, 956-961.
7. J. P. Rothstein, *Annu. Rev. Fluid Mech.* 2010, **42**, 89-109.
8. K. K. Varanasi, T. Deng, J. D. Smith, M. Hsu and N. Bhate, *Appl. Phys. Lett.* 2010, **97**, 234102.
9. J. Genzer and K. Efimenko, *Biofouling* 2006, **22**, 339-360.
10. P. M. Barkhudarov, P. B. Shah, E. B. Watkins, D. A. Doshi, C. J. Brinker and J. Majewski, *Corros. Sci.* 2008, **50**, 897-902.
11. X. Hong, X. Gao and L. Jiang, *J. Am. Chem. Soc.* 2007, **129**, 1478-1479.
12. P. Calvert, *Chem. Mater.* 2001, **13**, 3299-3305.
13. D. Ishii, H. Yabu and M. Shimomura, *Biostec.* 2010, **52,** 136-142.
14. C. W. Extrand, *Langmuir* 2002, **18**, 7991-7999.
15. G. McHale, N. J. Shirtcliffe and M. I. Newton, *Langmuir* 2004, **20**, 10146-10149.
16. N. J. Shirtcliffe, S. Aqil, C. Evans, G. McHale, M. Newton, C. C. Perry and P. Roach, *J. Micromech. Microeng.*2004, **14**, 1384-1389.
17. M. Nosonovsky, *Langmuir* 2007, **23**, 9919-9920.
18. L. Gao and T. J. McCarthy, *Langmuir* 2006, **22**, 6234-6237.
19. K. A. Wier and T. J. McCarthy, *Langmuir* 2006, **22**, 2433-2436.
20. D. Oner and T. J. McCarthy, *Langmuir* 2000, **16**, 7777-7782.
21. A. B. D. Cassie and S. Baxter, *Trans. Faraday Soc.* 1944, **40**, 546-551.
22. K. Sefiane, *J. Colloid Interface Sci.* 2004, **272**, 41.
23. S. L. Ceccio, *Annu. Rev. FluidMech.* 2010, **42**, 183-203.
24. T. Young, *Phil. Tran.* 1805, **95**, 65-87.

